

Unit cell dilation technique for analyzing dilatometry data

Nasseh Khodaie^{a*}, Douglas G. Ivey^b, Hani Henein^b

^aSchool of Advanced Technology, Algonquin college, Ottawa Canada K2G 1V8

^bDepartment of Chemical and Materials Engineering, University of Alberta, Canada T6G 2V4

*Corresponding author: +1 613 299 1817. E-mail address: khodain@algonquincollege.com

Keywords: Phase transformation kinetics; dilatometry; microalloyed steel

Abstract

Dilatometry is the most accurate and common method for measuring the kinetics of phase transformations in solid specimens. Despite the development of a more accurate technique, an inferior method, i.e., the lever rule, is widely used in the scientific community to interpret raw dilatometry data. This paper introduces a sound mathematical approach to modelling the physical phenomena of phase transformations, named continuous sequential phase transformation (CSPT). CSPT is used in creating an algorithm called unit cell dilation (UCD) that is used for analyzing the continuous phase transformation of two microalloyed steels. Results show that the UCD algorithm generates quantitative data for the phase content of the steel that is in good agreement with metallographic observations.

Introduction

The phase transformation of austenite in steels has been the subject of an enormous amount of research in the past 100 years. Despite a wealth of knowledge generated in this area, the key role of steel in heavy industries has fueled an ever increasing demand for better and cheaper steels. Central to this research, is the austenite phase transformation as it is the main phenomenon that greatly contributes to the mechanical properties of steel in all manufacturing techniques that involve heating of steel above its A_1 temperature.

Phase transformations are usually studied by subjecting a specimen to a designed thermal cycle, ideally in a controlled environment, using a thermal or thermo-mechanical simulator machine. The most useful and accurate method to study phase transformations is dilatometric analysis. In this technique, changes in the length (dilation) and

temperature of a specimen are recorded as a function of time. Subsequent analysis of the recorded data can reveal transformation start and finish temperatures without much processing, but the most valuable information that can be obtained by analyzing dilatometry data is the phase transformation kinetics. To measure the kinetics of a phase transformation, it is necessary to know the fractions of the phases during transformation. One method to calculate phase fractions from dilatometry data is the so called “lever rule”. It will be explained in detail that lever rule is not an adequate analysis method for complex phase transformation in steels and leads to predictable errors that can be mitigated using more sophisticated analysis techniques.

One of the milestones in any research field involving measurement of a physical phenomenon is the discovery of a reliable analysis technique coupled with an available and robust analysis tool for the obtained raw data. Historically, this has happened before in the fields of crystallography with the invention of Rietveld analysis as an analysis method for XRD raw data that laid the foundation for quantitative analysis of X-ray diffraction (XRD) and neutron diffraction patterns through full pattern analysis. This, in turn, led to the creation of tools such as GSAS [1] which is freely available for analysis of XRD patterns and serves as a benchmark for other quantitative XRD analysis software.

The goals of this paper are first to show the areas where the lever rule fails as an analysis technique and then to introduce a mathematical framework for analysis of dilatometry data, named “continuous sequential phase transformation” (CSPT). Finally, an algorithm named “unit cell dilation” (UCD) that implements the CSPT will be developed. This algorithm is used to develop computer codes “Fitter” and “Master Fitter” that carry on the computations and optimization of parameters, respectively. The authors envision that the UCD algorithm and the computer codes implementing it will become an easily accessible and standard analysis method for dilatometry experiments.

The lever rule

To begin, an understanding of the lever rule is essential and a review of how it is used will be presented. The lever rule is the easiest and most widely used method in interpreting dilatometry data. In the lever rule, it is assumed that the fraction of transformed parent phase is proportional to the distance of the dilation curve from extrapolated dilation lines of the phases before and after transformation, as shown in Figure 1 and Eq. 1.

$$f = \frac{a}{a + b} \quad \text{Eq. 1}$$

The lever rule has two major limitations. One is the inability of the lever rule to model sequential transformations. A sequential transformation occurs when the product of transformation is changed due to temperature or chemical changes in the parent phase. A sequential transformation commonly occurs during continuous cooling of most steels, except austenitic stainless grades. The two terms in Eq. 1 are defined with respect to the parent and the final product

microstructure. While the parent phase is usually single phase austenite, the product phase is a mixture of phases that formed during sequential phase transformation. In other words, Eq. 1 does not account for individual product phases but rather considers the combined effect of all phases after they have formed. Since Eq. 1 does not use any phase specific information when considering the products, the lever rule cannot account for sequential phase transformation and, by extension, any type of phase transformation that results in more than one phase. An experienced user, however, may be able to detect time and temperature of changes in transformation type by looking for deviations from trends in the cooling curves. However, as will be shown later in Figure 14, this method can result in considerable quantitative errors.

The second limitation is the inability of the lever rule to consider the effect of chemistry dependent (non-linear) properties for parent and product phases. This type of behavior occurs in steels when the diffusion controlled formation of ferrite results in the accumulation of carbon in austenite as the transformation progresses. The additional carbon, on one hand, reduces the coefficient of thermal expansion (CTE) of austenite and, on the other hand, causes the austenite lattice to stretch and expand to accommodate the carbon atoms. When the effect of these two phenomena on austenite is considered, it is concluded that the extrapolated γ line in Figure 1 cannot be a linear line as assumed by the lever rule, but has to tilt upwards (as shown by the dashed line in Figure 1) to reflect the lattice expansion and CTE reduction.

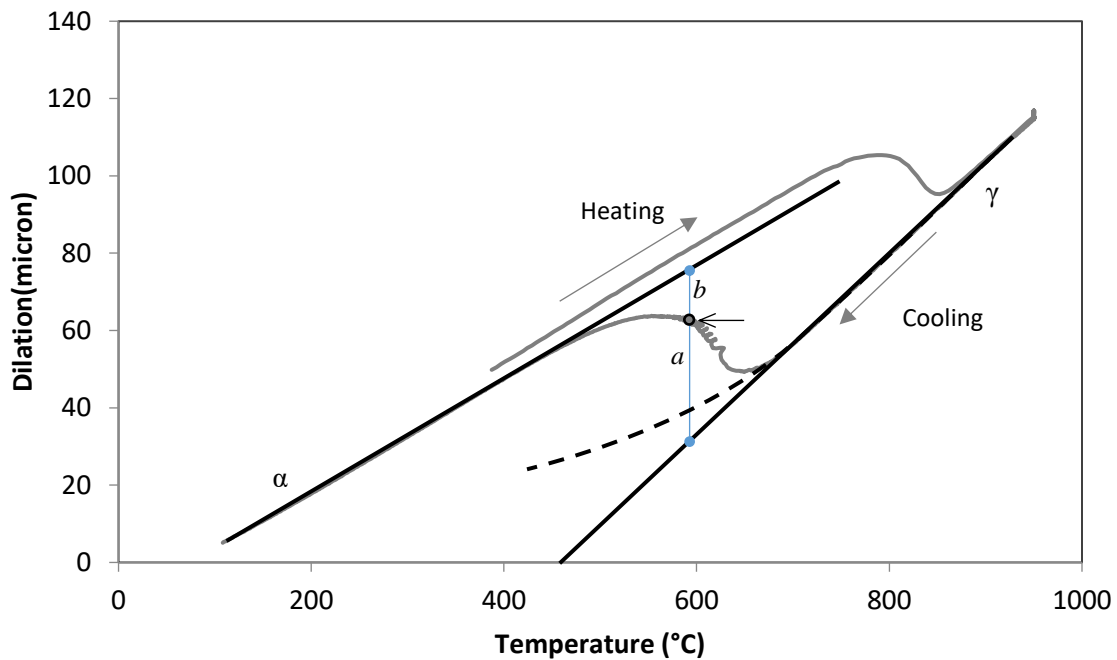


Figure 1. Example of dilatometry data for the austenite to ferrite transformation. The grey line is the actual dilatometer data and the black straight lines show the extrapolated austenite and ferrite dilation lines, as considered in the lever rule. The dashed line shows a schematic extrapolation of the austenite line, considering the effect of carbon accumulation in austenite.

There have been several successful attempts to address the shortcomings of the lever rule by calculating the volume change in the unit cell level [2–4]. The methods described by these papers address austenite enrichment and sequential transformation by making assumptions to simplify the mathematical solution process. As an example, Onink et al. [2] assume a uniform carbon concentration in the product, which is not generally the case, especially for bainite. This results in inaccurate estimation of the austenite carbon content, particularly for ultra-low carbon steel such as microalloyed steel where the steel’s carbon content is of the same order as the carbon solubility limit in ferrite (0.02 w%). The uniform ferrite carbon content assumption has been utilized in the work of many researchers relying on the calculations by Onink et al. [3–6]. The current work is an attempt to expand on Onink et al.’s work and provide a reliable algorithm and computational tool to implement this approach for microalloyed and possibly hypo-eutectoid steels.

Experimental procedure

The analysis of dilatometry data, obtained from an X80 steel during continuous cooling, is the subject of this paper. X80 steel is a pipeline steel with a yield strength of 80 ksi (550 MPa) as defined by API standards. The composition of this steel is shown in Table 1. The as received steel had a grain size of $3.1 \mu\text{m} \pm 0.6 \mu\text{m}$ on the surface normal to the width direction and $2.5 \mu\text{m} \pm 0.15 \mu\text{m}$ on the surface normal to rolling direction. The grain size was measured using the line intercept method according to ASTM E112 [7].

Table 1. Chemical composition (wt%) of the steel X80-N used in this study

C	Mn	Si	Cr+Ni+Mo+Cu	Nb	Ti	N
0.064	1.69	0.12	0.83	0.04	0.007	0.0064

To measure the kinetics of transformation, hollow, cylindrical samples measuring 4 mm OD, 3 mm ID and 10 mm in length were machined from the center of a 15 mm thick skelp with the length of the dilatometer sample in the rolling direction. Samples were then processed with a Bahr DIL 805 thermo-mechanical simulator. One experiment was done for each experimental condition. In the dilatometer, the samples were austenitized at 950°C for 15 minutes to ensure full transformation to austenite and then cooled at various rates ranging from 1°C/min to 40°C/min. The austenitizing temperature of 950°C was chosen to allow for partial dissolution of NbC to create an austenite chemistry similar to the austenite present after hot rolling and before transforming to ferrite. Figure 2 shows a schematic of the thermal cycles used in the dilatometer tests.

To observe the microstructures, following continuous cooling, samples were cut in half from the mid length to expose a circular cross section. Samples were then mounted, polished and etched using 2% Nital. Microstructural observation was done using a Hitachi S4800 field emission source scanning electron microscope (FE-SEM) operating in

secondary electron (SE) mode at 5 kV and a Leica DM ILM optical microscope using incandescent light with a blue filter. Quantitative metallography was performed to measure the volume fraction of microconstituents, using a point counting technique on 5 fields of view according to ASTM E562 [8].

To further test the accuracy of the developed codes, dilatometry data obtained for a steel, hereafter referred to as X80-K, is also analyzed. The raw dilatometry data is from Johnson et al. and the quantitative microstructural data is obtained from reference [9]. The chemical composition of steel X80-K is shown in Table 2. Steel X80-K was austenitized at 945°C for 5 minutes and cooled at constant cooling rates of 0.3°C/s, 0.5°C/s, 1°C/s, 5°C/s, 7°C/s, 10°C/s and 20°C/s to room temperature. The dilatometry samples were solid round bars with an OD of 6 mm and length of 10 mm. Dilatational measurements were taken from the diameter of the specimen. Metallographic analysis was done in reference [9] using both optical and scanning electron microscopy (SEM). Additional information about steel X80-K can be found in reference [9].

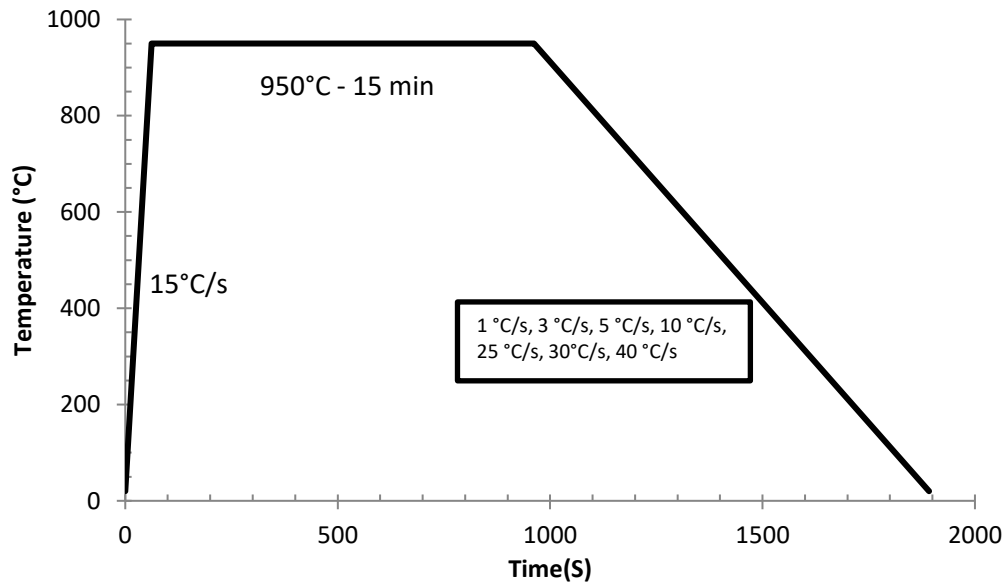


Figure 2. Schematic of thermal cycle used for the continuous cooling experiments.

Table 2. Chemical composition (wt%) of the X80-K steel used for validation

C	Mn	Si	Cr+Ni+Mo+Cu	Nb	Ti
0.058	1.65	0.25	0.73	0.091	0.016

Results

Dilatometry results obtained at different cooling rates are shown in Figure 3. To allow for better comparison between different cooling rates, all dilation data is normalized such that at 800°C the dilation is 0 μm . At higher cooling rates, the transformation begins and ends at lower temperatures. Even though all the cooling curves in this figure are normalized to begin from the same starting point, the graphs end up having a different dilation when the transformation is finished. These minor differences arise from a variation in the volume fraction of microconstituents in the final microstructure. The most notable is bainite/martensite (B/M) which contains retained austenite, which is the highest density phase in steels. The UCD algorithm automatically deals with these variations. Microstructural analysis of the samples processed using the dilatometer was done with an FE-SEM operating in SE mode. As examples, three micrographs are shown in Figure 4 to Figure 6. In these figures, QPF, DP, WF and BF represent quasi polygonal ferrite, degenerate pearlite, Widmanstatten ferrite and bainitic ferrite, respectively. Detailed description of the microconstituents and microstructures observed in the continuously cooled specimens can be found in [10].

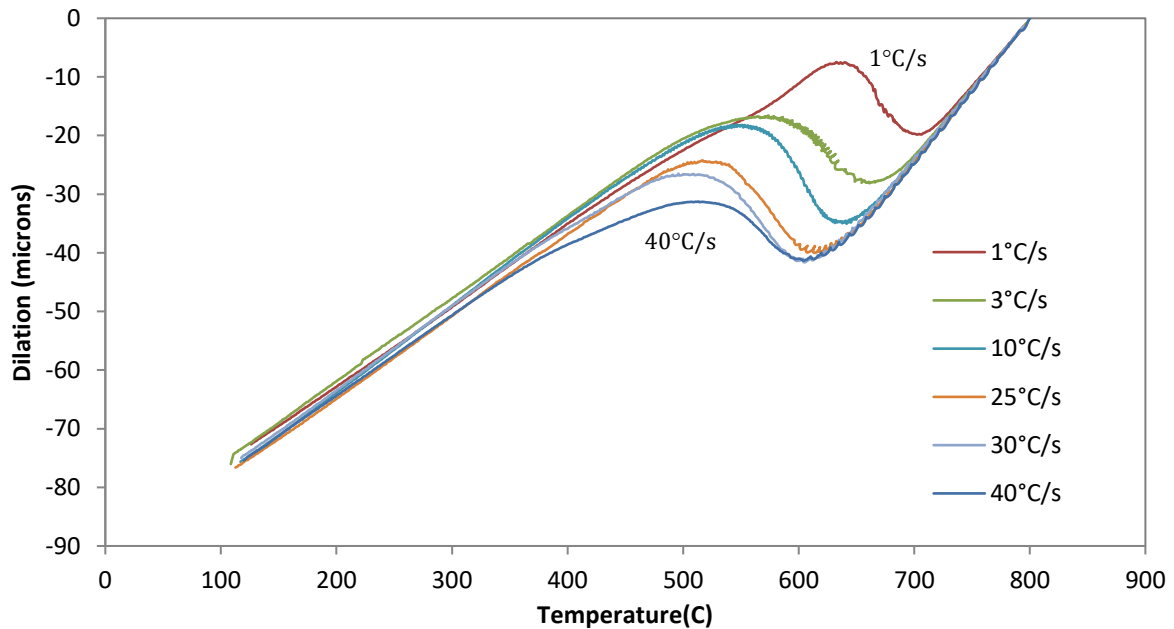


Figure 3. Normalized dilation graphs obtained at different cooling rates.

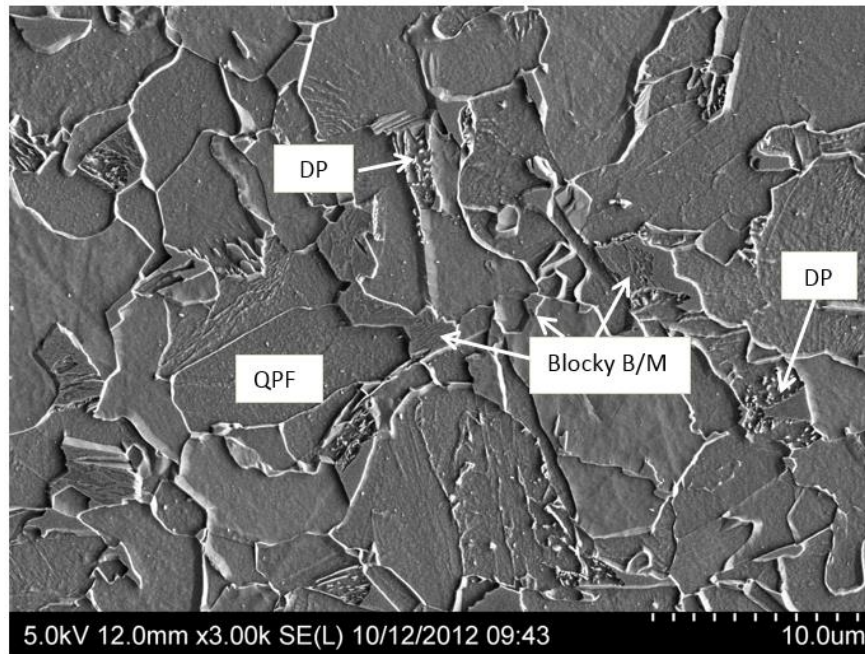


Figure 4. Microstructure of sample cooled at 1°C/s [10].

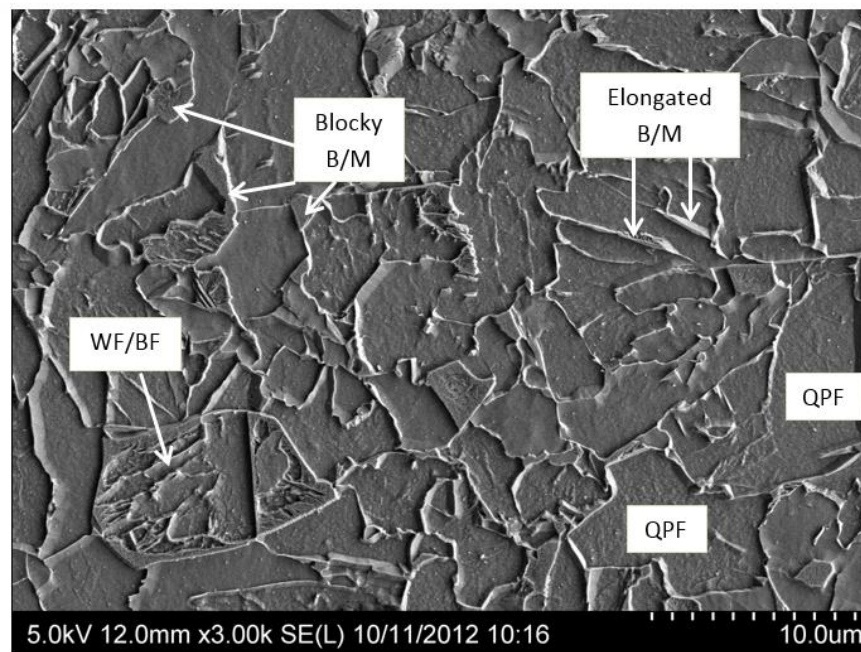


Figure 5. Microstructure of sample cooled at 10°C/s [10].

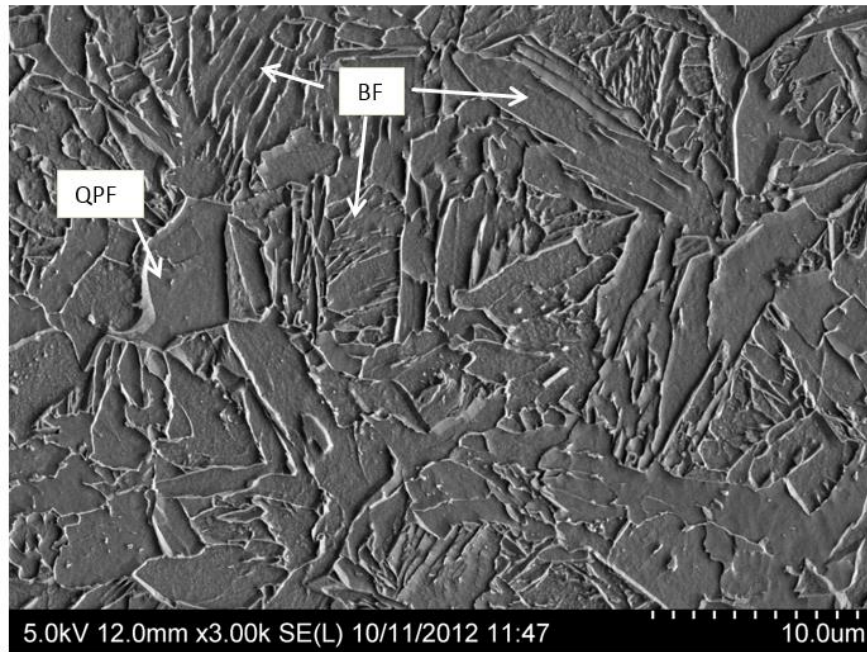


Figure 6. Microstructure of sample cooled at 40°C/s [10].

Quantitative metallography was done on the micrographs by measuring the volume fraction of three distinguishable groups of phases, i.e., ferrite group (QPF+BF), bainite and martensite group (B/M) and degenerate pearlite (DP). The volume fraction of QPF and BF are measured in combination, primarily because it was not possible to determine a phase boundary between them. A secondary reason is that BF can be easily mistaken for QPF if the BF plates are near parallel with surface. Both reasons are explained in detail elsewhere [10]. Quantitative metallography results measured for steel X80-N at different cooling rates, is shown in Figure 7.

Discussion

Continuous sequential phase transformation (CSPT)

As mentioned in the lever rule section, chemical changes can occur to the product and parent phases during transformation. As an example in steels, the amount of carbon dissolved in ferrite and austenite in the vicinity of the phase boundary is dictated by the thermodynamics and kinetics of the transformation. These concentrations are often calculated using the partitioning rule. There are several partitioning rules which are used depending on the kinetics on transformation; e.g., equilibrium for very slow transformations and para-equilibrium for relatively fast transformations. A common feature of these partitioning rules is that the amount of carbon in ferrite is temperature dependent and determined by the solvus line in the equilibrium or paraequilibrium phase diagram. For continuous cooling this results in chemical differences between the ferrite that forms at different temperatures. As a result, in non-isothermal phase

transformation of steel instead of having one ferrite phase, a non-uniform continuum of ferrite is created. The carbon concentration gradient in ferrite can be reduced by subsequent diffusion of carbon. However, this is only appreciable when diffusion domains are small (early stages of transformation or small prior austenite grain size) or when the transformation rate is slow. This is not, however, applicable for all transformations, especially for microalloyed steels with rapid transformation kinetics. It can be argued that carbon concentration changes are negligible for ferrite, but later it will be shown that considering a variable carbon content for ferrite opens the door for modeling BF and martensite as variants of ferrite. This method in defining PF, BF and martensite allows for considering the transition from one phase to another as a gradual process rather than an abrupt and discontinuous shift in the nature of the transformation.

To correctly address these issues, a new mathematical approach is required that allows for consideration of infinite sequential phase transformations. This approach must be able to (1) allow for formation of any number of phases, (2) allow for changes in the chemical composition of the product phase and take this effect into account and (3) determine the amount of the austenite consumed by the transformation by considering points (1) and (2). From an atomistic point of view, the total volume of a specimen can be calculated by summing the cell volume that each atom occupies, according to Eq. 2.

$$V = \sum_{i=1}^{N_{total}} v_i \quad \text{Eq. 2}$$

In this equation, v is the portion of the unit cell volume occupied by one atom (from now on referred to as volume per atom) and N_{total} is the total number of lattice atoms in the specimen. v is calculated by dividing the volume of a unit cell by the number of atoms in one unit cell. In this analysis only the number of atoms that make up the lattice structure of the phases are used in the calculations. The effect of interstitial atoms that are not part of the lattice structure is accounted for by considering their effect on the volume per atom of lattice atoms. Eq. 2 can be expanded by separating the volume of austenite from the products.

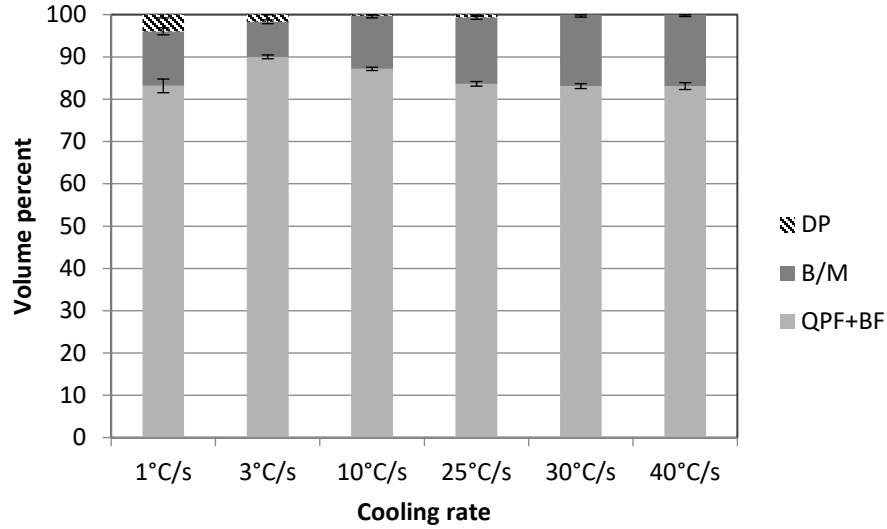


Figure 7. Measured volume fraction of microconstituents using point count technique on SEM micrographs.

Assuming the austenite phase has a uniform chemical composition, all the atoms in austenite can be assumed to be identical, so that Eq. 2 can be expanded as Eq. 3.

$$V = \sum_{i=1}^{N^p} v_i^p + N^\gamma \cdot v^\gamma \quad \text{Eq. 3}$$

The superscript p indicates the product phase, N^p is the number of product atoms, N^γ is the number of austenite atoms and v^γ is the volume per atom of austenite. Since the product volume is calculated by summation of very small quantities (volume per 1 atom) compared with the total product volume, the product volume term in Eq. 3 can be approximated using the integral function shown in Eq. 4.

$$\sum_{i=1}^{N^p} v_i^p \approx \int_0^{N^p} v^p dN^p \quad \text{Eq. 4}$$

Using Eq. 4, Eq. 3 can be written as Eq. 5.

$$V = \int_0^{N^p} v^p dN^p + N^\gamma \cdot v^\gamma \quad \text{Eq. 5}$$

Differentiating both sides of Eq. 5 turns it into an equation that can be solved using numerical methods such as finite difference; however, to correctly differentiate the equation in a way that represents the physical phenomenon of transformation, it is important to identify the independent variables and their effects on the terms in this equation. Both N^p and N^γ , the number of lattice atoms in the product phase and austenite, respectively, are ultimately functions of time. The volume per atom of product and austenite are functions of three variables, i.e., phase type, temperature and chemical composition. Chemical composition itself is a function of temperature (partitioning rule) and N^p (mass balance

of partitioned alloying elements). Since temperature is a time dependent variable and N^p is time dependent, all the variables in Eq. 5 can be expressed as time dependent functions. As a result, Eq. 5 needs to be differentiated with respect to time to model the physics of the transformation correctly (Eq. 6).

$$\frac{dV}{dt} = \frac{d}{dt} \left(\int_0^{N^p} v^p dN^p \right) + v^\gamma \cdot \frac{dN^\gamma}{dt} + N^\gamma \cdot \frac{dv^\gamma}{dt} \quad \text{Eq. 6}$$

The derivative of the integral term can be simplified by using Leibniz's rule [11]. The general form of this rule for a time dependent derivative is shown in Eq. 7.

$$\frac{d}{dt} \left(\int_{g(t)}^{h(t)} f(x, t) dx \right) = \int_{g(t)}^{h(t)} \frac{df(x, t)}{dt} dx + f(h(t), t) \cdot \frac{dh(t)}{dt} - f(g(t), t) \cdot \frac{dg(t)}{dt} \quad \text{Eq. 7}$$

Using this rule, Eq. 6 can be written as Eq. 8.

$$\frac{dV}{dt} = \int_0^{N^p} \left(\frac{dv^p}{dt} \right) \cdot dN^p + v^p \cdot \frac{dN^p}{dt} + v^\gamma \cdot \frac{dN^\gamma}{dt} + N^\gamma \cdot \frac{dv^\gamma}{dt} \quad \text{Eq. 8}$$

Eq. 8 may be explained phenomenologically as follows. The left hand side is the instantaneous rate of change in volume of the specimen. This change has four sources as shown in Eq. 8. The term $\int_0^{N^p} \left(\frac{dv^p}{dt} \right) \cdot dN^p$ calculates the instantaneous rate of change in volume that happened in the product phases that formed prior to time t. This includes mainly thermal contraction of the product phases, but can also include volume changes due to a chemical composition change of the product phase caused by a secondary process such as tempering or carbide precipitation. Hidden in the simplicity of this term is the fact that this integral assumes the product is made up of $\left(\frac{N^p}{dN^p} \right)$ product domains. These product domains can be completely different phases or the same phase with different chemical compositions. The contribution of each product domain to the overall volume change is calculated separately, which ensures that any number of phases could form. Thus, many sequential transformations and their effects are taken into account. In the next section this integral will be discretized over the product domain.

The term $v^p \cdot \frac{dN^p}{dt}$ calculates the rate of the change in volume created by the formation of a new product phase at time t. The term $v^\gamma \cdot \frac{dN^\gamma}{dt}$ calculates the rate of volume change that is caused by consumption of the austenite phase. The term $N^\gamma \cdot \frac{dv^\gamma}{dt}$ shows the rate of volume change that occurs in the austenite phase. The volume change in austenite has two equally important sources, i.e., temperature and chemical composition change caused by diffusive transformation and carbon accumulation.

Eq. 8 provides a robust framework for finding the number of austenite atoms that transform as a function of time. However, implementing a sound solution process depends heavily on the way v^p and v^γ are introduced to Eq. 8. As mentioned before, the volume per atom depends on the type of the phase, the temperature and the chemical

composition. Assuming that at a given time only one phase is forming (multiple phase transformations will be discussed later), the $\frac{dv}{dt}$ terms in Eq. 8 can be expanded to show the effect of these two parameters.

$$\frac{dv}{dt} = \left(\frac{\partial v}{\partial T} \Big|_{dM_i=0} \right) \cdot \frac{dT}{dt} + \sum_{i=C,Mn,Si\dots} \left(\frac{\partial v}{\partial M_i} \Big|_{dT=0} \right) \cdot \frac{dM_i}{dt} \quad \text{Eq. 9}$$

M_i is the concentration of element i in the phase. The concentration of elements in a phase depends on the partitioning rule that defines the proportion of concentrations in the product and austenite, but also depends on the mass balance between the two phases so that the net amount of alloying elements in the sample remains constant. Therefore, the dM_i terms are functions of dN_p which makes Eq. 8 a non-linear equation. As a result, the best way to solve Eq. 8 without compromising the number of variables to simplify the solution, is by numerical methods. This numerical solution, which is based on the finite difference technique, has been developed by the authors and is named Unit Cell Dilation (UCD).

UCD algorithm

Eq. 8 can be solved numerically by a time stepping finite difference technique. In this method, by stepping in time in small increments all the differential terms are estimated by simple algebraic expressions and solved using linear algebra methods. In general, between times i and $i + 1$, shown in Figure 8, Eq. 8 can be discretized according to Eq. 10.

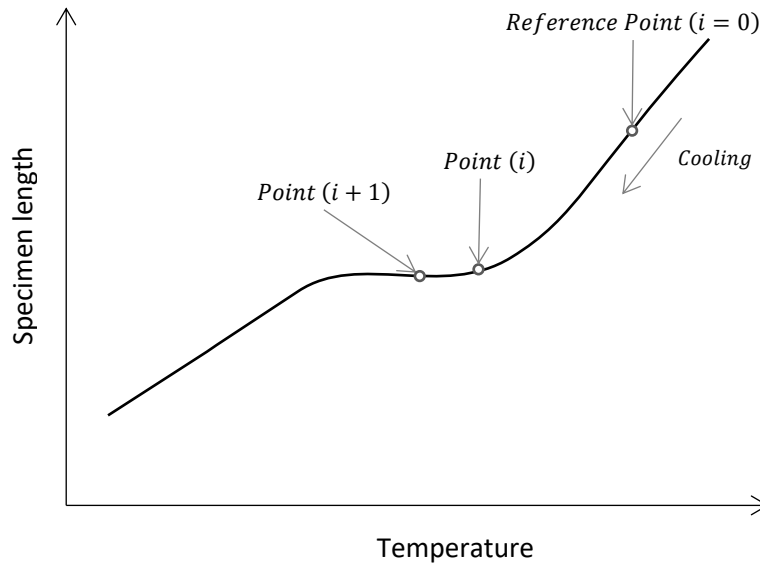


Figure 8. Sequential phase transformation of austenite to polygonal ferrite and bainitic ferrite.

$$\begin{aligned} \frac{(V_{i+1} - V_i)}{(t_{i+1} - t_i)} = & \sum_{j=0}^{i-1} \left[\frac{(v_{i+1}^p - v_i^p)}{(t_{i+1} - t_i)} \cdot (\Delta N_j^p) \right] + v_{(i+\frac{1}{2})}^p \cdot \frac{\Delta N_i^p}{(t_{i+1} - t_i)} - v_{(i+\frac{1}{2})}^y \\ & \cdot \frac{\Delta N_i^p}{(t_{i+1} - t_i)} + \left(N_{total} - \sum_{j=0}^{i-1} \Delta N_j^p - \Delta N_i^p \right) \cdot \frac{(v_{i+1}^y - v_i^y)}{(t_{i+1} - t_i)} \end{aligned} \quad \text{Eq. 10}$$

In Eq. 10, ΔN_k^p is the number of lattice atoms that have transformed to the product between steps k and $k + 1$, so that $N_{k+1}^p = N_k^p + \Delta N_k^p$. The term $v_{(i+\frac{1}{2})}^p$ indicates the volume per atom of the product at the mid-point between points i and $i + 1$. This is an estimation of the properties of the product while it is forming during one time step. Since the volume per atom is a function of chemical composition and temperature, $v_{(i+\frac{1}{2})}^p$ is calculated using the average temperature and average chemical composition between the points i and $i + 1$ as shown in Eq. 11.

$$v_{(i+\frac{1}{2})}^p = v^p \left(M = \frac{(M_i + M_{i+1})}{2}, T = \frac{(T_i + T_{i+1})}{2} \right) \quad \text{Eq. 11}$$

M shows the chemical composition, which includes the concentration of all the alloying elements in the alloy. Eq. 10 is an algebraic equation that can be solved numerically. However, calculation of ΔN_i^p is only possible if prior product type, chemical composition and amount at all prior steps are known. Therefore, the solution process has to begin from a reference point with a known microstructure and chemistry. The reference point can be easily set within the single phase austenite region during cooling, as shown in Figure 8 which serves as the initial condition for the solution.

To solve Eq. 10, it is necessary to know what phase or phases form during the time step. This can be done by using a program that compares the temperature and chemistry of austenite with predetermined conditions that trigger formation of a phase. As an example, before the calculation of the current time step begins, the martensite start temperature for austenite is calculated using an empirical model [12–14]. If the average temperature of the time step is lower than the calculated martensite start temperature for austenite, the product in that time step will be considered to be martensite and appropriate functions will be used in Eq. 10. The condition that triggers formation of bainite was investigated in [10] and the results showed that the empirical model developed by Lee et al. [5] performed better than the T'_0 method developed by Bhadeshia et al. [15]. The condition that triggers formation of cementite was considered to be equilibrium between austenite and cementite; i.e., exceeding the solubility limit of carbon in austenite would result in precipitation of cementite. Precipitation of cementite was considered to be immediate, which means the effect of kinetics on the volume fraction of precipitated cementite is not taken into account. Figure 9 shows the flowchart for the UCD algorithm.

Volume per atom

To be able to solve Eq. 10, it is necessary to have a reliable method to calculate the volume per atom of the phases participating in the transformation. For a crystalline phase, v can be calculated using Eq. 12.

$$v = \frac{\text{Volume of the unit cell}}{\text{Number of atoms in unit cell}} \quad \text{Eq. 12}$$

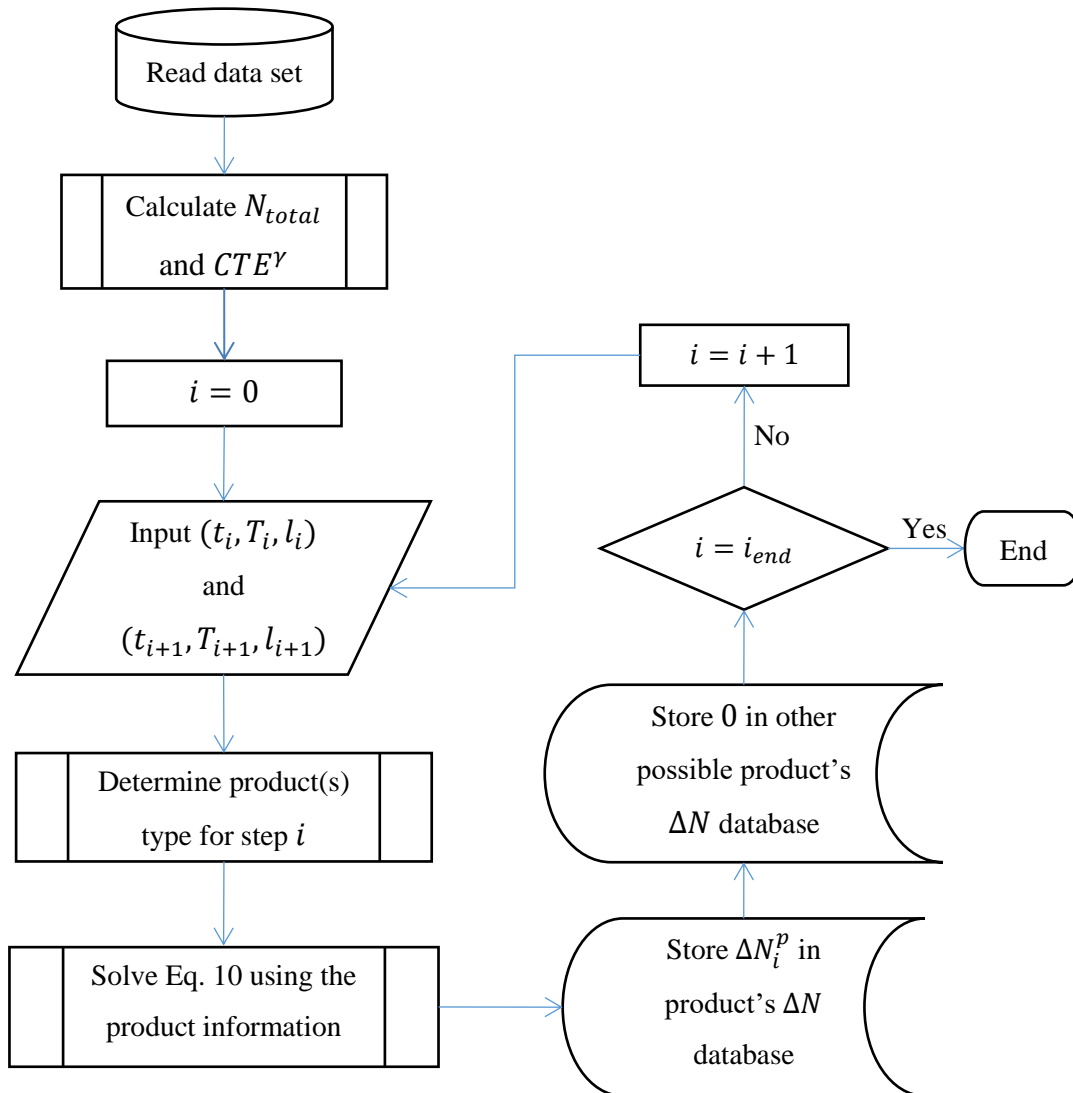


Figure 9. Flowchart for the UCD algorithm.

Austenite

The austenite unit cell has 4 atoms and its volume can be calculated using Eq. 13 to Eq. 15.

$$v_{unit\ cell}^{\gamma} = \left[a_{RT}^{\gamma} \left(1 + \int_{T=T_0}^T CTE^{\gamma} \cdot dt \right) \right]^3 \quad \text{Eq. 13}$$

$$a_{RT}^{\gamma} = a_0^{\gamma} + \sum_{j=C,Mn\dots} p_j c_j \quad \text{Eq. 14}$$

$$CTE^{\gamma} = CTE_0^{\gamma} + \sum_{j=C,Mn\dots} q_j c_j \quad \text{Eq. 15}$$

In these equations, a_0 is the lattice parameter at the reference temperature T_0 . It should be mentioned that the reference point for calculating the lattice parameter has nothing to do with the reference point selected for solving Eq. 10. To avoid confusion, the reference temperature for calculating the lattice parameter will be referred to as the lattice reference temperature. CTE_0 is the coefficient of thermal expansion when $c_j = 0$, i is the phase, c_j is the concentration of element j and p and q are the weighting factors for elements for the lattice parameter and CTE, respectively. The p_j and q_j factors can be found in the literature [5,16–18]; however, some partitioning rules such as para-equilibrium assume zero partitioning for substitutional elements, which means their concentration in the product and austenite is always the same as the nominal steel composition. This allows for simplification of Eq. 13 through Eq. 15 by just calculating the change caused by partitioning of carbon (and nitrogen if not negligible).

Ferrite and Ferrite Derivatives (FD)

From a crystallographic point of view, the lattice for bainitic ferrite and martensite is, in fact, an extension of the ferrite lattice for pure iron with added strain due to dissolved carbon and/or nitrogen (if present). When the amount of dissolved carbon is less than 0.6 wt%, the FD unit cell is cubic or near cubic. At higher carbon contents, the body centered cubic unit cell changes to a body centered tetragonal type by stretching the unit cell in the c direction while slightly shrinking it in the a direction [19,20]. Table 3 shows the variation in lattice parameters of ferrite derivatives at room temperature as a function of carbon content.

Table 3. Change in lattice parameter of ferrite derivatives as a function of carbon content.

C (wt%) < 0.6	C (wt%) > 0.6
$a_{RT}^{FD}(\text{Å}) = a_0^{\alpha}(\text{Å}) + W_{a.low\ C}^{FD} \cdot C$	$a_{RT}^{FD}(\text{Å}) = a_0^{\alpha}(\text{Å}) + W_{a.high\ C}^{FD} \cdot C$
$c_{RT}^{FD} = a_{RT}$	$c_{RT}^{FD} = a_0^{\alpha}(\text{Å}) + W_{c.High\ C}^{FD} \cdot C$

$W_{a.low\ C}^{FD}$ is the carbon weight factor for lattice parameter (a) at low carbon content, $W_{a.high\ C}^{FD}$ is the carbon weight factor for lattice parameter (a) at high carbon content and $W_{c.High\ C}^{FD}$ is the carbon weight factor for lattice parameter (c) at high carbon content. a_0^{α} can be calculated as a function of concentration of elements other than carbon in the phase,

as explained by Lee et al. [16] or measured experimentally and calculated by subtracting effect of carbon using the equations shown in Table 3. The unit cell volume of ferrite derivatives can be calculated using Eq. 16 and Eq. 17 [5].

$$v_{unit\ cell}^{FD} = \left[a_{RT}^{FD} \left(1 + \int_{T=T_0}^T CTE^{FD} \cdot dt \right) \right]^2 \cdot \left[c_{RT}^{FD} \left(1 + \int_{T=T_0}^T CTE^{\alpha} \cdot dt \right) \right] \quad \text{Eq. 16}$$

$$CTE^{FD} = CTE_0^{FD} + CTE_1^{FD} \cdot T + CTE_2^{FD} \cdot T^2 - CTE_3^{FD} \cdot C \quad \text{Eq. 17}$$

C is the carbon content in at%, T is the temperature in °C and CTE_i^{FD} are the polynomial constants. Using Eq. 16 and Eq. 17, three microconstituents, i.e., (quasi) polygonal ferrite, bainitic ferrite and martensite, can be modelled and used in Eq. 10. The carbon content of the FD phase has an important role in defining its true nature and properties. The lowest carbon content in a FD phase belongs to polygonal ferrite (PF). The carbon content of PF during transformation is determined by the partitioning rule. The most commonly used partitioning rule for microalloyed steels is para-equilibrium; therefore, it is the one used in this study. The carbon content assigned to FD according to para-equilibrium is the maximum thermodynamically stable amount of carbon that can dissolve in an FD phase. However, the highest amount of carbon in an FD phase occurs for martensite, which inherits all the carbon in austenite. Between the two extremes of carbon content in the FD phase, there is a situation where FD receives more carbon than the para-equilibrium content but less than the full austenite carbon content. This applies to bainitic ferrite and is explained in the following section.

Carbon content of FD

The amount of carbon dissolved in bainitic ferrite is more than the para-equilibrium content [21,22]. According to the displacive theory of bainite formation, bainitic ferrite initially receives all the carbon atoms in austenite; however, during the pause needed for recovery of austenite, some of this carbon escapes back to austenite [21,23] resulting in partial supersaturation. To model partial supersaturation of carbon in FD, it is useful to define a supersaturation fraction (SSF) as Eq. 18.

$$SSF = \frac{M_C^{FD} - M_{C,PE}^{FD}}{M_C^Y - M_{C,PE}^{FD}} \quad \text{Eq. 18}$$

M_C^{FD} is the observed concentration of carbon in the FD phase, $M_{C,PE}^{FD}$ is the concentration of carbon in FD according to para-equilibrium and M_C^Y is the concentration of the carbon in the austenite phase. SSF=1 means that all the carbon in austenite is inherited by FD, which applies to martensite. SSF=0 corresponds to $M_C^{FD} = M_{C,PE}^{FD}$, which means the amount of carbon dissolved in the FD phase is equal to the amount allowed by para-equilibrium; in other words, no supersaturation occurs. This applies to PF and QPF.

Rearranging Eq. 18 to calculate the amount of carbon in FD results in Eq. 19, which is used in the UCD algorithm.

$$M_C^{FD} = SSF(M_C^Y - M_{C,PE}^{FD}) + M_{C,PE}^{FD} \quad \text{Eq. 19}$$

$M_{C,PE}^{FD}$ can be calculated using thermodynamic databases such as Thermo-Calc. The SSF is a function of chemical composition and temperature and can be calculated by measuring the carbon content in bainitic ferrite using atom probe tomography [22,24] or XRD [22]. When SSF data is not available, SSF may be approximated as a linear function between values of zero and one at the lower bainite start temperature (LBs) and Ms temperature.

Cementite

Cementite has an orthorhombic unit cell with 12 iron atoms per unit cell. Its unit cell volume can be calculated using Eq. 20.

$$v^{cem.} = abc \times ((1 + 5.311 \times 10^{-6} - 1.942 \times 10^{-9}T + 9.655 \times 10^{-12}T^2)(T - 293))^3 \quad \text{Eq. 20}$$

$a = 0.45234 \times 10^{-9}(m)$, $b = 0.50883 \times 10^{-9}(m)$ and $c = 0.67426 \times 10^{-9}(m)$.

Multiple phase transformation

Multiple phase transformation refers to simultaneous formation of two or more phases. As an example in steels, the transformation to pearlite is a multiple phase transformation of ferrite and cementite. Multiple phase transformation of cementite and FD phases are implemented in the UCD algorithm by evaluating the austenite-cementite equilibrium in the product type subroutine. If the amount of carbon in austenite exceeds the solubility limit of austenite, cementite will be allowed to form along with the FD phase. The amount of cementite that forms depends on the amount of FD phase formed at the current step, which is yet to be determined by the solver subroutine. When cementite formation is triggered, ΔN_i^p in Eq. 10 is replaced by $\Delta N_i^{FD} + \Delta N_i^{cem}$, which adds another unknown to Eq. 10. As a result, there has to be another equation relating ΔN_i^{FD} and ΔN_i^{cem} to allow for a unique solution. The second equation can be written by considering the mass balance of carbon between FD, cementite and austenite. Assuming that the carbon content of austenite after formation of cementite is equal to the solubility limit, the mass balance equation can be written as Eq. 21.

$$\begin{aligned}
& \left(N_{total} - \sum_{i=0}^{i-1} \Delta N_i^p \right) \left(\frac{C_{i-1}^\gamma}{1 - C_{i-1}^\gamma} \right) \\
& = \Delta N_{i-1}^{FD} \cdot \left(\frac{C_i^{FD}}{1 - C_i^{FD}} \right) + \Delta N_{i-1}^{cem} \cdot \left(\frac{1}{3} \right) \\
& + \left(N_{total} - \sum_{i=0}^{i-1} \Delta N_i^p - \Delta N_{i-1}^{FD} - \Delta N_{i-1}^{cem} \right) \cdot \left(\frac{C_i^\gamma}{1 - C_i^\gamma} \right)
\end{aligned} \tag{Eq. 21}$$

C^γ is the atomic fraction of carbon in austenite and C^{FD} is the atomic fraction of carbon in FD. The left hand side of Eq. 21 shows the amount of carbon in austenite before formation of the products in the current step. The right hand side sums up the amount of carbon in FD, cementite and austenite after formation of the product. By solving Eq. 10 and Eq. 21 as a set, the amount of ΔN_{i-1}^{FD} and ΔN_{i-1}^{cem} can be calculated.

This approach to model multiple phase transformations is different than the work by Onink et al. [2] and Lee et al. [5], because independent formation of cementite is permitted here which allows for simultaneous modelling of the multiple phase transformation of pearlite (mixture of polygonal ferrite and cementite) and upper bainite (mixture of bainitic ferrite and cementite).

Implementation of UCD algorithm

The UCD algorithm is just a numerical approach, which needs proper implementation to work correctly. The implementation was done by designing two programs named “Fitter” and “Master Fitter”. The Fitter program applies UCD to one experimental data file consisting of time, temperature and dilation data. It uses the Nelder-Mead simplex minimization technique to find the molar fraction of product formed during one time step, by minimizing a cost function. The cost function in the Fitter program, is the sum of absolute value of the difference between the dilation calculated using the amount of product formed and the experimentally measured dilation at analysis points. By minimizing this difference the Fitter program ensures that the fraction transformed during each time step creates the expected dilation to match the experimental data.

The Fitter program relies on the user provided data about the material and phase properties which will be referred to as material parameters. These parameters are used to model the volume of the phases as explained in the volume per atom section. The Fitter program begins from a point with known phase content, usually austenite before the transformation begins, and then moves to the next point and calculates the phase content needed to make the modeled dilation equal to the experimentally measured value. Although possible, considering all of the collected point in a data file to perform the UCD calculations is not practical as speed of calculation declines exponentially as number of analyzed points increase. Therefore a method must be used to pick only important points among in the raw data file. This task is assigned to a program called “Data File conditioner”. Data File Conditioner selects a point by comparing it with the last selected point using a criterion. This criterion can be defined using time, temperature or dilation of the point or a

combination of them. A time base criterion to keep constant Δt between selected points creates a different number of analysis points depending on the cooling rate, which is fine for the Fitter Program but proved to be problematic for the Master Fitter program which will be introduced later. A temperature based criterion is impractical as it would neglect all the points during isothermal periods of the thermal cycle. A dilation based selection criterion seems to be the most reliable as it is the dilation of the points that is the subject of UCD calculations. However, a functional dilation based selection criterion that works the same way regardless of the cooling rate and transformation temperature has not been found by the authors yet. The main hurdle in implementing a dilation based criterion is the fact that dilation caused by transformation depends on the temperature of the parent and product phases which at this point are not known yet. Therefore the same amount of dilation would translate into different amounts of phase transformation for different experiments. This would cause the same problem as using constant Δt as the selection criterion, i.e., hugely different numbers of analysis points for different experiments.

To address the issues of the mentioned selection criteria, a hybrid time and temperature based selection criterion is used. In this method a point is selected for analysis if 10 s is passed ($\Delta t = 10 \text{ s}$) or the temperature is changed by 3°C ($\Delta T = 3^\circ\text{C}$) compared with the last selected point. The choice of ΔT and Δt is arbitrary and can be changed by the user. These conditions ensure that a proper number of data points are selected during both the isothermal and continuous cooling parts of a dilatometry experiment. The selected points are then stored in a new data file named “conditioned data file”. The points that do not make the selection process to be considered in the conditioned data file are used for reducing the noise in dilation and temperature of the selected point using a polynomial fit.

To allow the user to reduce the number of analysis point further, there is an option of selecting all the points in the conditioned data file or selecting 1 of every n points. The n parameter, which is referred to as the “interval”, is user defined and can be any natural number. The points that are not considered in the final calculations are used for noise reduction using a polynomial fit. The combined effect of the hybrid selection process and the interval is that at cooling rates below 0.3°C/s there is $10n$ (s) time difference between the selected points and for cooling rates higher than 0.3°C/s there is $3n$ ($^\circ\text{C}$) temperature difference between the selected points with n being the interval. The mentioned strategies allow the Master Fitter program to use variable time steps to treat the different experiments with relatively equal weight in its analysis.

As mentioned, the Fitter program uses material properties such as CTE and unit cell parameters to calculate the fraction of phases during transformation. Some of these material parameters can be measured directly from the experimental dilatometry data. As an example, CTE^γ can be measured experimentally since there is a temperature range, after the austenitization period and before the onset of transformation, where the microstructure is completely austenitic. During this period, the CTE of the whole specimen is equal to CTE^γ at the nominal steel composition. The property that is measured specifically for a phase in the material of interest provides the most reliable source of data for modeling that phase, considering the experimental error is negligible. However, not all material parameters can be

measured for a specific specimen, because a single phase microstructure in the specimen is unlikely to happen. For instance, in low alloy and carbon steels, the ferrite phase is always accompanied by cementite and/or austenite. To measure CTE^{α} one would need to create a new specimen that has the identical chemical composition to the original specimen with its carbon content reduced to the solubility limit of ferrite. While it is possible to do so, for example, by decarburizing the specimen in a controlled oxidative atmosphere, from a practical point of view this does not seem to be a solution available for every dilatometry experiment. Therefore, it is necessary to use existing developed models to calculate the material parameters under different thermal and chemical conditions. These models provide a reliable way to estimate the material parameters; however, to obtain the best results using UCD, the error arising from the use of the non-customized constants must be minimized. This was the reason for writing the second program named “Master Fitter”. This program is written to fine tune the material parameters.

The Master Fitter program finds the best combination of material parameters by analyzing a dataset rather than one data file at a time. A dataset is collection of data files obtained for the same material. In a nutshell, Master Fitter runs the Fitter program on a dataset obtained under different conditions, such as cooling rate, using only one set of material parameters and then quantitatively evaluates the Fitter program for all the experiments. This is done by using either one of the two optimization algorithms implemented in the Master Fitter program. One of the optimization algorithms uses the differential evolution technique to do a global minimization to find the best combination of parameters within a defined range for each parameter. The other one uses the Nelder-Mead simplex minimization technique starting from a user defined initial guess for the optimized parameters. Differential evolution is more reliable than Nelder-Mead in finding the best answer, but it is a much slower search algorithm compared with Nelder-Mead.

Both optimization techniques find the best parameters by minimizing a cost function. The cost function of Master Fitter is a quantitative measure of how “good” the calculated fraction of the product is at the analyzed points. The unique feature about Master Fitter is that it determines the so-called goodness of the output of the Fitter program the same way that a human would do, by analyzing the shape of graph of the fraction transformed vs temperature for continuous cooling or the time for isothermal transformation. In human terms, a “good” result must meet the following 5 criteria.

1. At the end of the cooling cycle where the transformation is stopped, the phase fraction of products must remain constant.
2. The calculated dilation, using the material parameters, should match the experimentally measured dilations before, during and after the transformation.
3. The fraction of transformation must not exceed 1.
4. To ensure a correct fit, calculated dilations at the end of a cooling cycle must match experimental data. This is helpful since the errors for all previous analysis points accumulate and become pronounced at the point near the end of the cooling cycle.

5. The maximum amount of transformation should occur.

The first criterion is implemented by calculating a cost function as the difference between the slope of fraction transformed vs temperature $\left(\frac{df}{dT}\right)$ and the ideal end slope of 0. The cost function for the second criterion is calculated by summing the absolute value of the difference between the calculated dilation and the measured dilation for all the analysis points. Since the fraction transformed is calculated in steps, it is possible the sum of the fraction transformed exceeds one, which obviously is incorrect. To prevent this from happening, the third criterion is defined. The cost function for the third criterion is calculated by examining all the analysis points and issuing a large error for points that exceed a fraction transformed of 1. This large error ensures that the third criterion outweighs the other criteria and is always met. The fourth criterion is implemented similar to number two. The fifth criterion is implemented by calculating the cost function as the sum of the absolute value of the difference between the fraction transformed of the end points and the target fraction transformed of 1. The fifth criterion is optional and is only used when the optimization algorithm tries to meet the other four criteria by increasing the lattice parameter of ferrite, which reduces the fraction transformed to numbers close to zero. This criterion ensured that the optimization algorithm finds solutions that involve highest amount of transformation possible. The Master Fitter program then calculates an overall cost for every experiment by linearly adding all the 5 costs using Eq. 22.

$$\text{cost for one experimental data} = \sum_{i=1}^5 W_i \cdot \text{cost}_i \quad \text{Eq. 22}$$

In this equation W_i is the user defined weighting factor assigned to the cost function i . By changing the weight factors, the user can alter the influence of each cost function on overall cost. This allows for better accommodation of the experimental results obtained for various types of steels and instruments. After calculating the cost for each and every experimental data file, the overall cost of the dataset is calculated by adding the cost calculated for each experiment.

Convergence

The UCD algorithm is essentially a 2-dimensional time-marching finite difference method in which X (molar fraction transformed) is calculated as a function of time by estimating the derivatives over discrete time steps as shown in Eq. 10. Similar to all finite difference techniques, estimated derivatives become more accurate as the time step becomes smaller and the numerical answer of the differential equation converges to the exact solution. However, this increased accuracy comes at a minor price of speed and computation time, but more importantly at a possible cost of instability and loss of convergence. Therefore, the UCD algorithm needs to be checked for convergence. Since the exact solution of the fraction transformed as a function of time is not known, the only way to check for convergence is to analyze the results as the time step become smaller. In the current implementation of the UCD algorithm, the time step is replaced with a parameter called interval. Figure 10 shows the results of the Fitter program on the experimental data obtained at

5°C/s as a function of temperature using different intervals. As Figure 10 shows, the fraction transformed plots converge to the result obtained at the smallest time step, i.e., interval 1. This is especially visible in the temperature range of 550°C to 450°C.

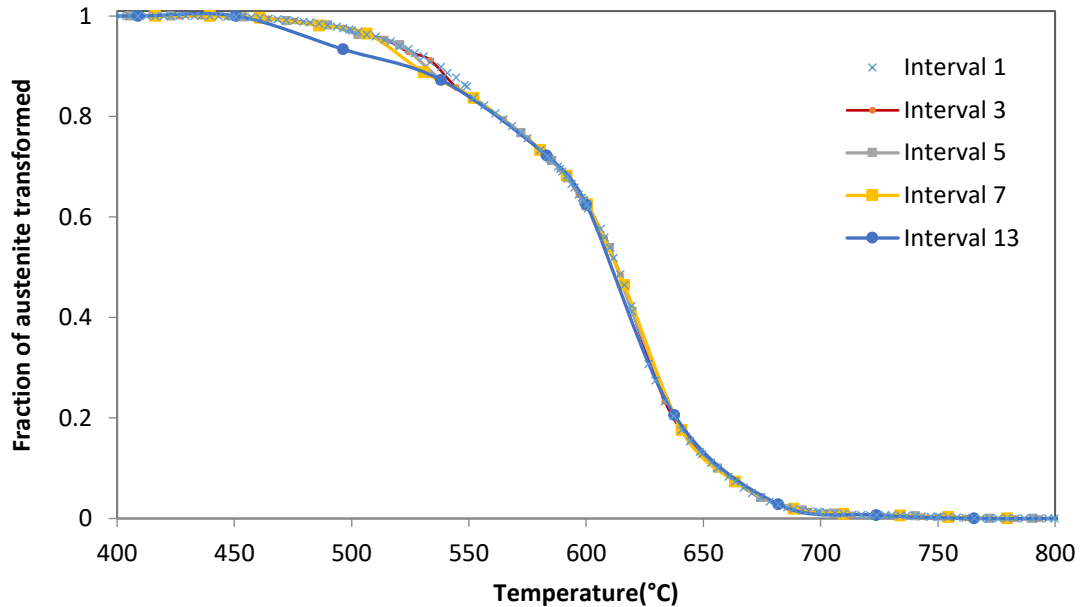


Figure 10. Fraction transformed as a function of temperature calculated using different intervals at the cooling rate of 5°C/s. Smaller intervals mean smaller time steps. This figure shows that the UCD algorithm results converge as the time step become smaller.

Validation of the UCD algorithm

Steel X80-N

To validate the UCD algorithm, dilatometry data obtained from a series of continuous cooling experiments performed on a X80 microalloyed steel were analyzed using the UCD algorithm and the results are compared with the measurements done using quantitative metallography. Figure 11 shows the phase content calculated by the UCD algorithm for the steel X80-N. This figure shows that while the trend in change of QPF and BF is as expected, the amount of B/M stays relatively unchanged at $14.6\% \pm 1.7\%$. The underlying reason for such behavior is unclear for the authors. Figure 12 shows a comparison of the volume fractions of microconstituents measured metallographically with the calculated ones using the UCD algorithm. Except for the amount of pearlite, the UCD calculations are within 5% of the metallographic measurements. Although the Fitter and Master Fitter programs are capable of detecting pearlite, the code did not detect the formation of pearlite. This may be due to uncertainty in the definition of the carbon solubility limit in ferrite and austenite. Further analysis with higher carbon steels is needed to address this issue properly. The material parameters were optimized using the Master Fitter program. These parameters are shown in the **Error!** **Reference source not found..**

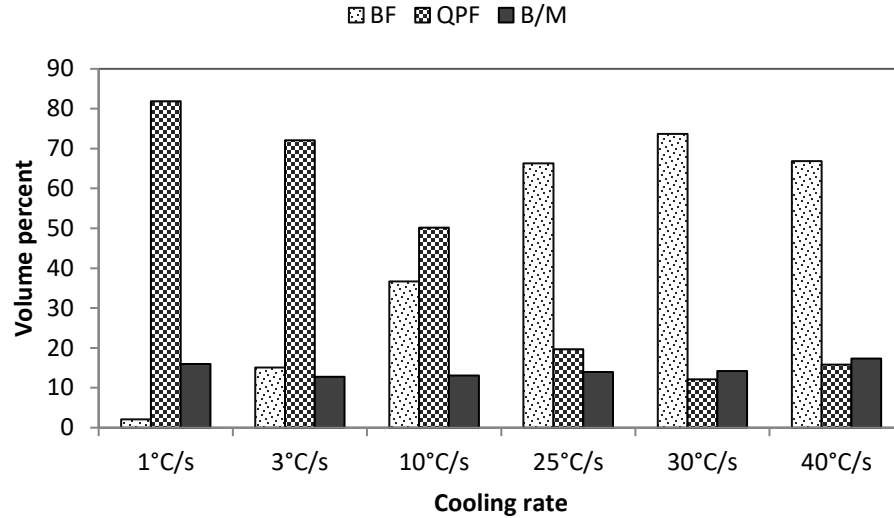


Figure 11. Phase content of steel X80-N calculated by the Master Fitter program.

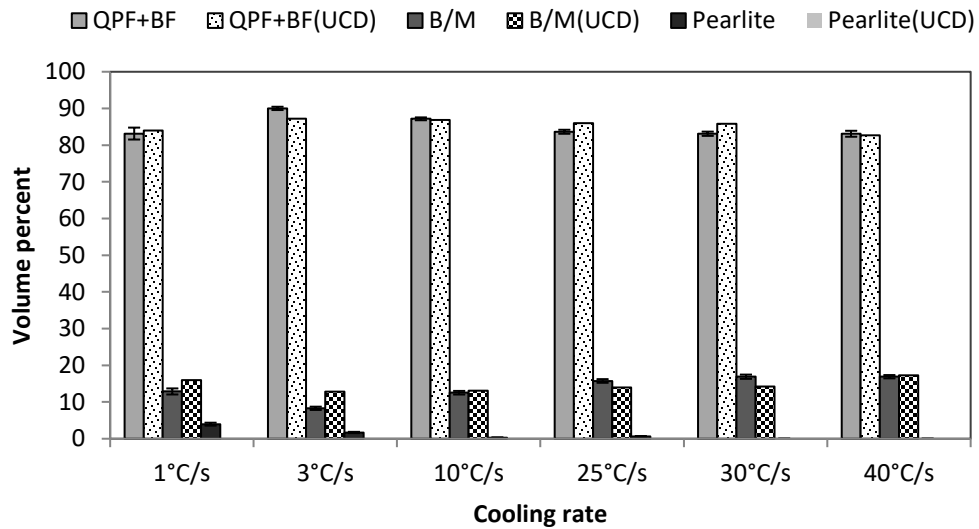


Figure 12. Comparison of calculations made using the UCD algorithm with quantitative metallography measurements for steel X80-N.

Figure 13 shows the variation in lattice parameter of austenite as a function of temperature during cooling for three cooling rates of 1°C/s, 10°C/s and 40°C/s. Before the transformation begins, the carbon content of austenite is constant; therefore, the lattice parameter is only a function of temperature with the slope of line being proportional to CTE^{γ} . This, however, changes at lower temperatures. As transformation begins at lower temperatures, formation of ferrite results in accumulation of carbon in austenite which, on one hand, results in swelling of the austenite unit cell

causing upward deviation from the linear trend. On the other hand, carbon accumulation in austenite results in a reduction of CTE^γ which also causes an upward deviation from the linear trend seen before transformation begins.

Table 4. Material parameters used by the Fitter program before and after optimization by the Master Fitter*.

Microconstituent	Application	Before optimization	After optimization
Austenite	Eq. 14	$a_0^\gamma = 0.36306 \text{ nm}$ at $T_0 = 726.85^\circ\text{C}$ [3]	$a_0^\gamma = 0.36304 \text{ nm}$ at $T_0 = 726.85^\circ\text{C}$
Ferrite Derivatives (FD)	Table 3	$a_0^\alpha = 0.28610 \text{ nm}$ at $T_0 = 0^\circ\text{C}$ [5] $W_{a.low\ c}^{FD} = 0.02$ $W_{a.high\ c}^{FD} = 0.013 \times 10^{-10}$ $W_{c.high\ c}^{FD} = 0.116 \times 10^{-10}$	$a_0^\alpha = 0.286304 \text{ nm}$ at $T_0 = 20^\circ\text{C}$ $W_{a.low\ c}^{FD} = 0.026$ $W_{a.high\ c}^{FD} = 0.013 \times 10^{-10}$ $W_{c.high\ c}^{FD} = 0.116 \times 10^{-10}$
	Eq. 17	$CTE_0^{FD} = 1.1712 \times 10^{-5} \text{ k}^{-1} \dagger$ $CTE_1^{FD} = 1.3290 \times 10^{-8} \text{ k}^{-2} \dagger$ $CTE_2^{FD} = -8.9475 \times 10^{-12} \text{ k}^{-3}$ [25] † $CTE_3^{FD} = 1.9 \times 10^{-4} \text{ k}^{-1}$ [5]	$CTE_0^{FD} = 1.273 \times 10^{-5} \text{ k}^{-1}$ $CTE_1^{FD} = 4.822 \times 10^{-9} \text{ k}^{-2}$ $CTE_2^{FD} = 0 \text{ k}^{-3}$ $CTE_3^{FD} = 2.52 \times 10^{-4} \text{ k}^{-1}$

* Shaded parameters were not optimized as they were not used in the calculations.

† Calculated using the CTE data for pure ferrite presented in reference [25].

The upward deviation continues until the concentration of carbon in austenite reaches the solubility limit of carbon in austenite with respect to cementite. From this point, the carbon content of austenite is determined by the solubility limit function. In the absence of redistribution of substitutional atoms, the solubility limit becomes exclusively a temperature dependent function. Therefore, after the onset of cementite precipitation, the lattice parameter of austenite is the same for all cooling rates. This is the reason all three curves follow the same path after the arrows that indicate the point where the solubility limit is reached in austenite.

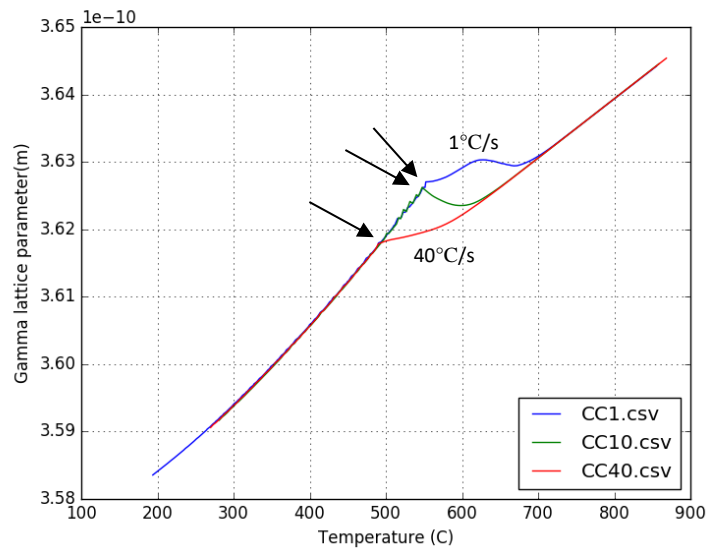


Figure 13. Lattice parameter of austenite as a function of temperature at different cooling rates. Arrows show the point at which the carbon content of austenite begins following the solubility limit of carbon in austenite with respect to cementite.

Benchmarking the performance of the UCD algorithm against the lever rule is of value. For this purpose, the dilatometry data obtained at the cooling rate of 1°C/s , analyzed using the two methods, is compared. As mentioned earlier, the lever rule does not account for sequential phase transformation. However, some dilatometry plots may contain clues that indicate sequential phase transformation. One of the indicators is the formation of a linear line in the dilation vs temperature graph, between two curved regions. The entry point to the linear region is the end of the first phase transformation and the exit point from the linear region is the beginning of the second phase transformation. A linear region can only be clearly observed when there is a period between the two phase transformations where no transformation occurs, which is not a general case for all sequential phase transformations. Nevertheless, examining Figure 3 shows that when comparing all the cooling rates, only the dilatometry plot obtained for continuous cooling at 1°C/s shows a sign of sequential phase transformation. For clarity, the dilation curve obtained for 1°C/s is shown alone in Figure 14. It can be seen that during cooling two transformation ranges exist that are separated by the straight part of the cooling curve shown by the dashed line. Judging by the difference in the amount of dilation observed for these two transformations, it is expected that the product of the first transformation has a higher volume fraction compared with the secondary phase transformation. Figure 15 shows volume fraction of transformed austenite calculated using the lever rule and the UCD algorithm as a function of temperature for a cooling rate of 1°C/s . Phase fractions calculated using the lever rule show that the linear region occurs at 90% phase transformation, while metallographic measurement shows the volume fraction of the major phase (polygonal ferrite) is 82%. In comparison, UCD calculates the volume fraction of the polygonal ferrite as 83%, which matches the 82% value measured using quantitative metallography. Figure 16 shows a comparison of phase content calculated using the lever rule and measured using quantitative metallography. For cooling rates more than 1°C/s , since no obvious changes were seen in the cooling curves, all the

product is assumed to be single phase PF. By comparing Figure 12 and Figure 16 it is evident that UCD not only outperforms the lever rule in analyzing multi-phase microstructures, but makes more accurate predictions for phase contents.

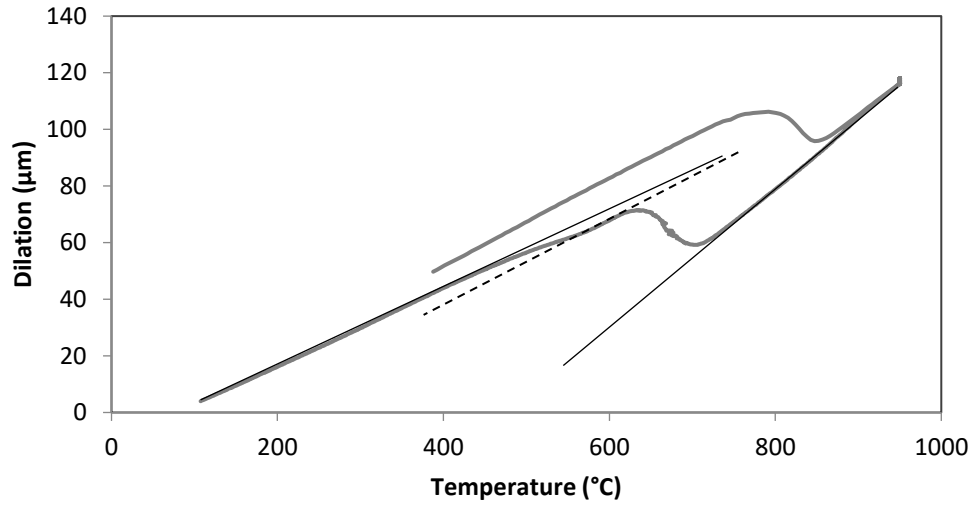


Figure 14. Continuous cooling at 1°C/s. Sequential phase transformation is confirmed by the formation of a linear region (dashed line) at about 600°C.

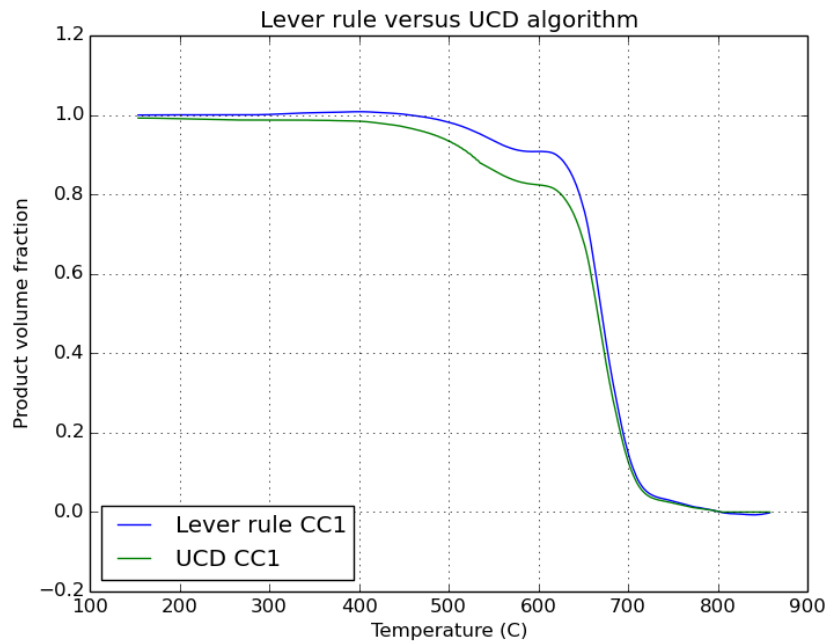


Figure 15. Product volume fraction vs temperature at 1°C/s calculated using UCD and the lever rule.

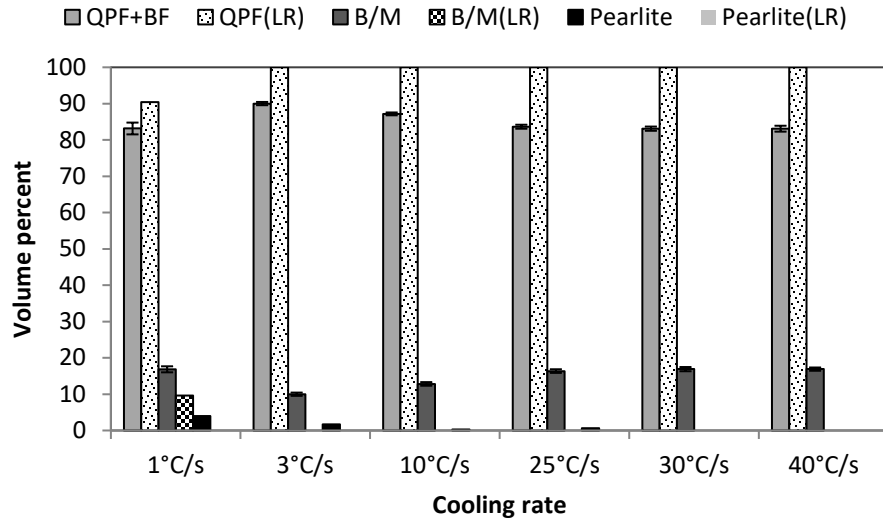


Figure 16. Comparison of calculations made using the lever rule with quantitative metallography measurements for steel X80-N. LR indicates lever rule.

Steel X80-K

To further test the validity of the developed algorithm and codes, a dataset containing dilatometry data for continuous cooling experiments on an X80 steel was obtained from reference [9]. The raw dilatometry data is analyzed using the Master Fitter program. Table 5 shows the material parameters calculated by the optimization program.

Table 5. Material parameters used by the Fitter program before and after optimization by Master Fitter*.

Microconstituent	Application	Before optimization	After optimization
Austenite	Eq. 14	$a_0^\gamma = 0.36306 \text{ nm}$ at $T_0 = 726.85^\circ\text{C}$ [3]	$a_0^\gamma = 0.36304 \text{ nm}$ at $T_0 = 726.85^\circ\text{C}$
Ferrite Derivatives (FD)	Table 3	$a_0^\alpha = 0.28610 \text{ nm}$ at $T_0 = 0^\circ\text{C}$ [5] $W_{a.low c}^{FD} = 0.02$ $W_{a.high c}^{FD} = 0.013 \times 10^{-10}$ $W_{c.high c}^{FD} = 0.116 \times 10^{-10}$	$a_0^\alpha = 0.286168 \text{ nm}$ at $T_0 = 20^\circ\text{C}$ $W_{a.low c}^{FD} = 0.058$ $W_{a.high c}^{FD} = 0.013 \times 10^{-10}$ $W_{c.high c}^{FD} = 0.116 \times 10^{-10}$
	Eq. 17	$CTE_0^{FD} = 1.1712 \times 10^{-5} \text{ k}^{-1} \dagger$ $CTE_1^{FD} = 1.3290 \times 10^{-8} \text{ k}^{-2} \dagger$ $CTE_2^{FD} = -8.9475 \times 10^{-12} \text{ k}^{-3}$ [25] † $CTE_3^{FD} = 1.9 \times 10^{-4} \text{ k}^{-1}$ [5]	$CTE_0^{FD} = 1.274 \times 10^{-5} \text{ k}^{-1}$ $CTE_1^{FD} = 5.641 \times 10^{-9} \text{ k}^{-2}$ $CTE_2^{FD} = 0 \text{ k}^{-3}$ $CTE_3^{FD} = 3.54 \times 10^{-4} \text{ k}^{-1}$

* Shaded parameters were not optimized as they were not used in the calculations.

† Calculated using the CTE data of pure ferrite presented in reference [25].

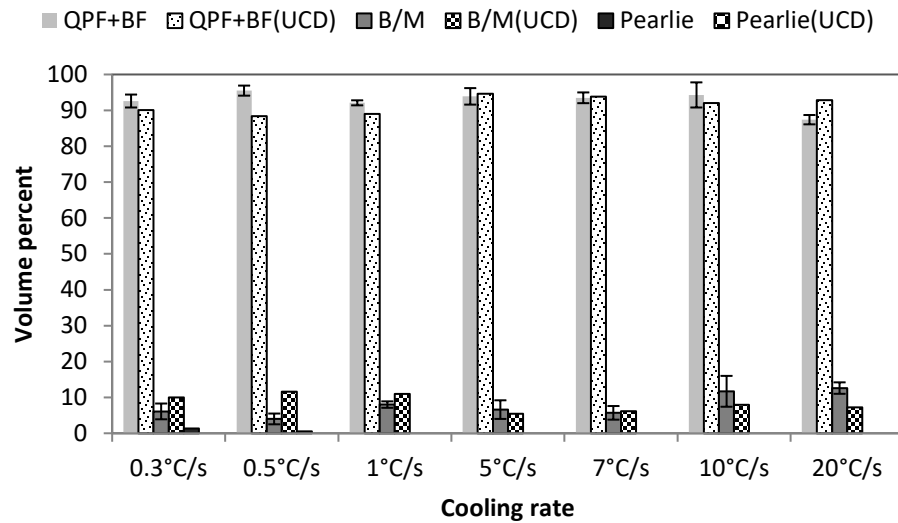


Figure 17. Comparison of calculations made using the UCD algorithm with quantitative metallography measurements for steel X80-K. Reproduced with permission from [9].

Figure 17 shows a comparison of the phase fractions calculated using the UCD algorithm and metallographic measurements. Aside from the cooling rate 0.5°C/s , at all cooling rates good agreement is observed between the Master Fitter results and metallographic measurements of phase content. The main reason for the poor fit for a cooling rate of 0.5°C/s is the odd trend that is observed in CTE^{γ} during cooling. Theoretically the CTE of a phase is only a function of its state variables, namely chemical composition, phase type, temperature and pressure. However, as shown in Figure 18, CTE^{γ} for steel X80-K appears to be a function of cooling rate. Such a trend was not observed for steel X80-N.

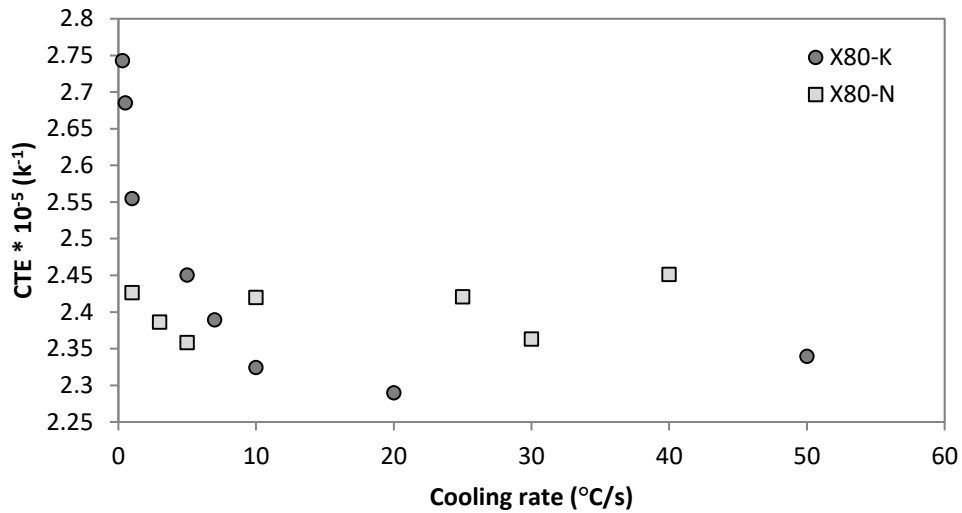


Figure 18. CTE of austenite during cooling after austenitization for steels X80-K and X80-N.

The dependence of CTE^γ on cooling rate may be a result of specimen creep under the force of the extensometer. This hypothesis agrees with the reduction in CTE^γ to expected values at higher cooling rates. At low cooling rates, the strain rate due to temperature reduction becomes small enough to be comparable with the small creep strain rate caused by the force applied by the extensometer. For steel X80-K, dilatometry was done using a Gleeble machine on a solid sample with dilatational measurements taken on the diameter of the specimen [9]. The extensometer force, no matter how small, can translate into a large stress when divided by a small contact area on the surface of specimen. For steel X80-N, dilatational measurements were taken on the length of the specimen which increases the contact area between the extensometer and the specimen.

To accommodate the observed variability of CTE^γ among different specimens of a dataset, the Fitter and Master Fitter programs allow for this material parameter to be different for each experiment. This is done by calculation of CTE^γ and N_{total} at the beginning of the calculations using the pure austenite portion of cooling curve. Until a better method is found to account for the differences in CTE^γ for different cooling rates involving steels with the same chemical composition, this seems to be the only way of handling this issue.

Conclusions

Using the lever rule to analyze dilatometry data for diffusive phase transformations can give rise to errors that could be prevented by considering the effect of redistribution of the alloying elements on the unit cell volume of the phases. This approach, originally established by Onink et al., is further developed in this study by introducing the concept of continuous sequential transformation, which assumes that the product phase is always changing. Also, multiple phase transformations are modelled in a new way, which considers the transformation as a cooperative but independent

development of two microconstituents, i.e., ferrite derivative (FD) and cementite. Each of these microconstituents form under their own thermodynamic constraints. This allows for efficient modeling of pearlite, bainitic ferrite, upper bainite, lower bainite and martensite using just one model.

All the new adjustments were implemented in an algorithm called unit cell dilation (UCD) which is used for creating two computer codes called the Fitter and the Master Fitter. The accuracy of the two programs was verified by comparing the results of two sets of dilatometry experiments with metallographic measurements of phase content.

Acknowledgements

The authors would like to acknowledge the support of the Natural Sciences and Engineering Research Council (NSERC) of Canada, Evraz Inc. NA, TransCanada PipeLines Ltd., Enbridge, Alliance Pipelines, UT Quality, the Resource for the Innovation of Engineered Materials program at Canmet MATERIALS of Natural Resources Canada (particularly Dr. Fateh Fazeli and Dr. Benoit Voyzelle) and Dr. Mehdi Towhidi for his invaluable help with the Python programming language.

References

- [1] A.C. Larson, R.B. Von Dreele, General Structure Analysis System (GSAS), Los Alamos Natl. Lab. Rep. LAUR. 748 (2004).
- [2] M. Onink, F.D. Tichelaar, C.M. Brakman, E. Mittemeijer, S. van der Zwaag, Quantitative Analysis of the Dilatation by Decomposition of Fe-C Austenites ; Calculation of Volume Change upon Transformation, *Z. Met.* 87 (1996) 24–32.
- [3] T.A. Kop, J. Sietsma, S. Van Der Zwaag, Dilatometric analysis of phase transformations in hypo-eutectoid steels, *J. Mater. Sci.* 36 (2001) 519–526.
- [4] L. Zhao, Quantitative dilatometric analysis of intercritical annealing in a low-silicon TRIP steel, *J. Mater. Sci.* 37 (2002) 1585–1591.
- [5] S.-J. Lee, M.T. Lusk, Y.-K. Lee, Conversional model of transformation strain to phase fraction in low alloy steels, *Acta Mater.* 55 (2007) 875–882. doi:10.1016/j.actamat.2006.09.008.
- [6] M. Jung, S.-J. Lee, Y.-K. Lee, Microstructural and Dilatational Changes during Tempering and Tempering Kinetics in Martensitic Medium-Carbon Steel, *Metall. Mater. Trans. A.* 40 (2009) 551–559. doi:10.1007/s11661-008-9756-2.
- [7] ASTM standard - E112 Standard Test Methods for Determining Average Grain Size, ASTM International, 2003.
- [8] ASTM standard E562 - Standard Test Method for Determining Volume Fraction by Systematic Manual Point Count, ASTM International, 2003.
- [9] K. Jonsson, Modification of the Stress-Strain Curve for High-Strength Line Pipe Steel, University of Alberta, 2013. <https://era.library.ualberta.ca/public/view/item/uuid:7287b2cf-0b84-4168-838e-ff9edb3d5405/>.
- [10] N. Khodaie, D.G. Ivey, H. Henein, Extending an empirical and a fundamental bainite start model to a continuously cooled microalloyed steel, *Mater. Sci. Eng. A.* 650 (2016) 510–522. doi:10.1016/j.msea.2015.10.016.
- [11] W. Kaplan, *Advanced Calculus*, Redwood City, Calif. : Addison-Wesley, Advanced Book Program, 1991.
- [12] K.W. Andrews, *Empirical Formulae for the Calculation of Some Transformation Temperatures*, J. Iron Steel Inst.

203 (1965) 721–727.

- [13] C. Capdevila, F.G. Caballero, C.G. de Andrés, Determination of martensite-start temperature in steels: Bayesian neural network model, *ISIJ Int.* 42 (2002) 894–902.
- [14] W.G. Vermeulen, P.F. Morris, A.P. de Weijer, S. van der Zwaag, Prediction of martensite start temperature using artificial neural networks, *Lronmaking Steelmak.* 23 (1996) 433–437.
- [15] H.K.D.H. Bhadeshia, D.V. Edmonds, The mechanism of bainite formation in steels, *Acta Metall.* 28 (1980) 1265–1273. doi:10.1016/0001-6160(80)90082-6.
- [16] S.-J. Lee, Y.-K. Lee, Quantitative analyses of ferrite lattice parameter and solute Nb content in low carbon microalloyed steels, *Scr. Mater.* 52 (2005) 973–976. doi:10.1016/j.scriptamat.2005.01.028.
- [17] M. Onink, C.M. Brakman, F.D. Tichelaar, E.J. Mittemeijer, S. van der Zwaag, J.H. Root, et al., The lattice parameters of austenite and ferrite in Fe-C alloys as functions of carbon concentration and temperature, *Scr. Metall. Mater.* 29 (1993) 1011–1016.
- [18] N.N. Rammo, O.G. Abdulah, A model for the prediction of lattice parameters of iron–carbon austenite and martensite, *J. Alloys Compd.* 420 (2006) 117–120. doi:10.1016/j.jallcom.2005.10.075.
- [19] L. Xiao, Z. Fan, Z. Jinxiu, Z. Mingxing, Lattice-parameter variation with carbon content of martensite. I. X-ray-diffraction experimental study, *Phys. Rev. B.* 52 (1995) 9970–9978. <http://journals.aps.org/prb/abstract/10.1103/PhysRevB.52.9970> (accessed September 30, 2014).
- [20] O.D. Sherby, J. Wadsworth, D.R. Lesuer, C.K. Syn, The c/a Ratio in Quenched Fe-C and Fe-N Steels - A Heuristic Story, *Mater. Sci. Forum.* 539-543 (2007) 215–222. doi:10.4028/www.scientific.net/MSF.539-543.215.
- [21] S.A. Mujahid, H.K.D.H. Bhadeshia, Coupled diffusional/displacive transformations: Effect of carbon concentration, *Acta Metall. Mater.* 41 (1993) 967–973. doi:10.1016/0956-7151(93)90031-M.
- [22] F.G. Caballero, M.K. Miller, C. Garcia-Mateo, Carbon supersaturation of ferrite in a nanocrystalline bainitic steel, *Acta Mater.* 58 (2010) 2338–2343. doi:10.1016/j.actamat.2009.12.020.
- [23] S.A. Mujahid, H.K.D.H. Bhadeshia, Partitioning of carbon from supersaturated ferrite plates, *Acta Metall. Mater.* 40 (1992) 389–396. doi:10.1016/0956-7151(92)90313-4.
- [24] F.G. Caballero, M.K. Miller, C. Garcia-Mateo, J. Cornide, M.J. Santofimia, Temperature dependence of carbon supersaturation of ferrite in bainitic steels, *Scr. Mater.* 67 (2012) 846–849. doi:10.1016/j.scriptamat.2012.08.007.
- [25] L.R. Smith, W.C. Leslie, Properties of Pure Metals, Properties and Selection: Nonferrous Alloys and Special-Purpose Materials, in: *ASM Handb. Vol. 2*, ASM International, 1990: pp. 1099–1201.